LHCb 98-006 TRIG
22 January 1998

The L1 Vertex Trigger Algorithm and its Performance

H. Dijkstra and T. Ruf
CERN, CH-1211 Geneva 23, Switzerland

Abstract

A distinctive signature of the desired signal events of the LHCb experiment are the number of displaced secondary vertices. In order to exploit this feature in the LHCb trigger, a special vertex detector had been designed to allow a fast online track reconstruction with a high precision and a high efficiency. A basic description of the vertex trigger algorithm proposed for the LHCb experiment is given in this note.

1 Introduction

The vertex processor analyses events after the level 0 decision at an incoming event rate of $1\,\mathrm{MHz}$. The input to the vertex processor are the r and ϕ cluster centers of the vertex detector. The latency foreseen at the moment is $256\,\mu$sec.

B-mesons with their decay products within the acceptance of the spectrometer are produced with a polar angle typically below 200 mrad, hence the projection of the impact parameter of the decay products to the primary vertex in the rz-plane is large, while the distribution of the projection in the plane perpendicular to the beam-axis is nearly compatible with tracks originating from the primary vertex.

The fast track reconstruction uses first the information of the r detectors only. This gives with sufficient precision the position of the primary vertex in space and allows a selection of tracks with a significant impact parameter to this vertex. Only to those tracks, the information of the ϕ detectors is added. A secondary vertex search is started looking for combinations of pairs of tracks which are close in space. Finally the trigger decision is based on the number of vertices found and on their distance to the primary vertex.

All results of this note had been obtained using the standard LHCb Monte-Carlo programme (SICB V113).

2 Choice of the Vertex Detector Geometry

The operation of the track and vertex finding algorithm is greatly simplified if the silicon detectors follow an r,ϕ geometry:

- Seeds for the track finding are located in the 12 inner ϕ sectors. The average charge track multiplicity in each of these sectors is about 1 (Fig. 1), which limits the number of hit combinations to be tried.
- To first order the r-coordinates define the z-position of the vertices.

The silicon detectors of the LOI, with strips along the x- and y-coordinates, are replaced by silicon detectors with similar resolutions but with strips at constant radius r from the beam axis and separated in 6 (12 for the inner r-detectors) ϕ sectors. This new geometry has in addition the advantage of a more flexible design with respect to the optimisation of the algorithms. Thus, for example, the strip pitches can be adapted to the resolution and occupancy requirements, which depend mainly upon the radius. Also it allows to divide the track finding into independant, parallel running parts for each of the separate ϕ sectors in a natural way.

2.1 Layout of the r,ϕ Silicon Vertex Detector

The 17 detector stations are placed along the beam axis in such a way that every track, which comes from the primary or a secondary vertex and is within the spectrometer

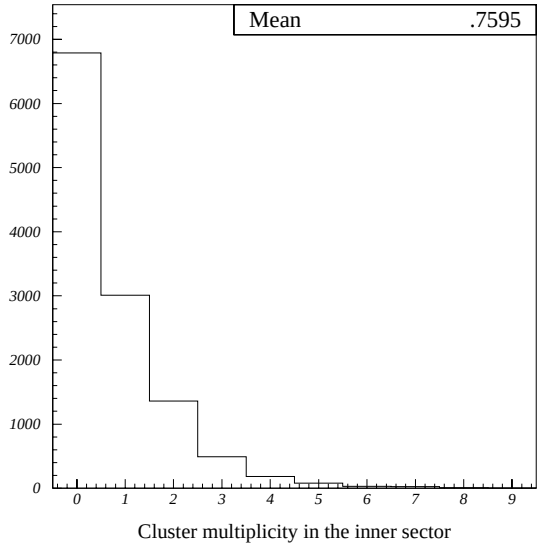

Figure 1: The cluster multiplicity in one inner silicon sector.

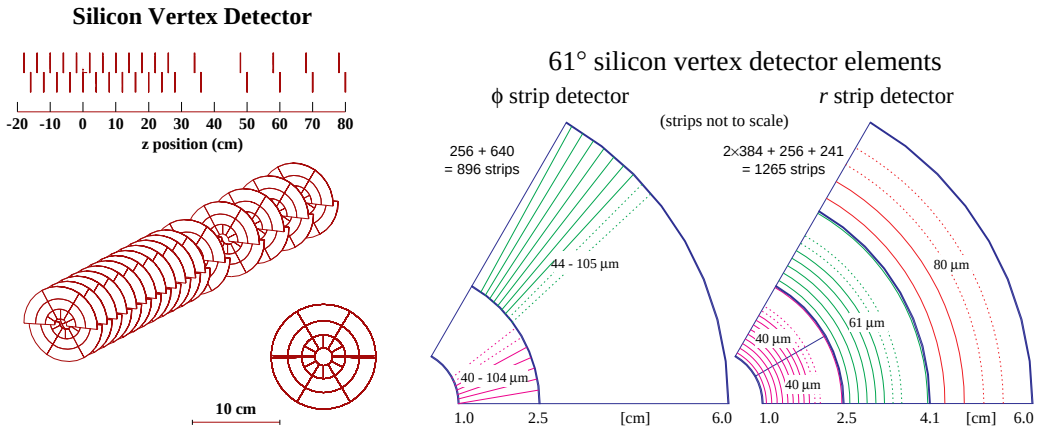

Figure 2: The vertex detector setup along the beam axis together with the individual ϕ and r detectors.

Table 1: Dimensions of the silicon vertex detector

r-detector			
radius	strip pitch	coverage	channels
$1.0 - 2.536$ cm	40 μm	30.5°	2×384
-4.072 cm	60 μm	61°	256
-6.000 cm	80 μm	61°	241
ϕ-detector			
radius	strip pitch	coverage	channels
$1.0 - 2.536$ cm	$40 - 104$ μm	61°	256
-6.000 cm	$41 - 98$ μm	61°	640

acceptance, hits at least two planes of the vertex detector. One vertex detector station consists of 6 ϕ sectors (61°) with two planes, which are sensitive to r and ϕ coordinates respectively (Fig. 2). The overlap of top and bottom stations, which are separated by 2 cm in z, of 3°, allows a fast online alignment.

The r detector has strips at constant radius, starting at 1 cm distance from the beam up to 6 cm, with strip pitches of 40, 60 and 80 μm. The division into inner, middle and outer sections was motivated by the fact that any track inside the spectrometer acceptance has to have at least one a hit in the silicon detector at a radius $r < 2.5$ cm, and that the measurement accuracy of this first point has the major effect on the resolution of the z coordinate of the vertex position. The inner section is again divided into two 30.5° sectors in order to make the track finding simpler avoiding hit ambiguities.

The precise ϕ coordinates of a track are measured by silicon detectors with strips arranged almost radially. The strips are tilted by some small angle ($\pm 5^\circ$ for consecutive stations) to resolve ambiguities when combining the r and ϕ information. Strip pitches range from 40 μm to 104 μm.

2.2 Simulation

All simulations are done using the standard LHCb Monte-Carlo (SICB) which is based on the GEANT package. Details about the simulation of the vertex detector response, the digitisation and the reconstruction of clusters can be found in ref. [1].

3 The L1 Vertex Trigger Algorithm

3.1 Overview

The algorithm consists of five consecutive parts (see also Fig. 3):

- Track finding in the r-projection

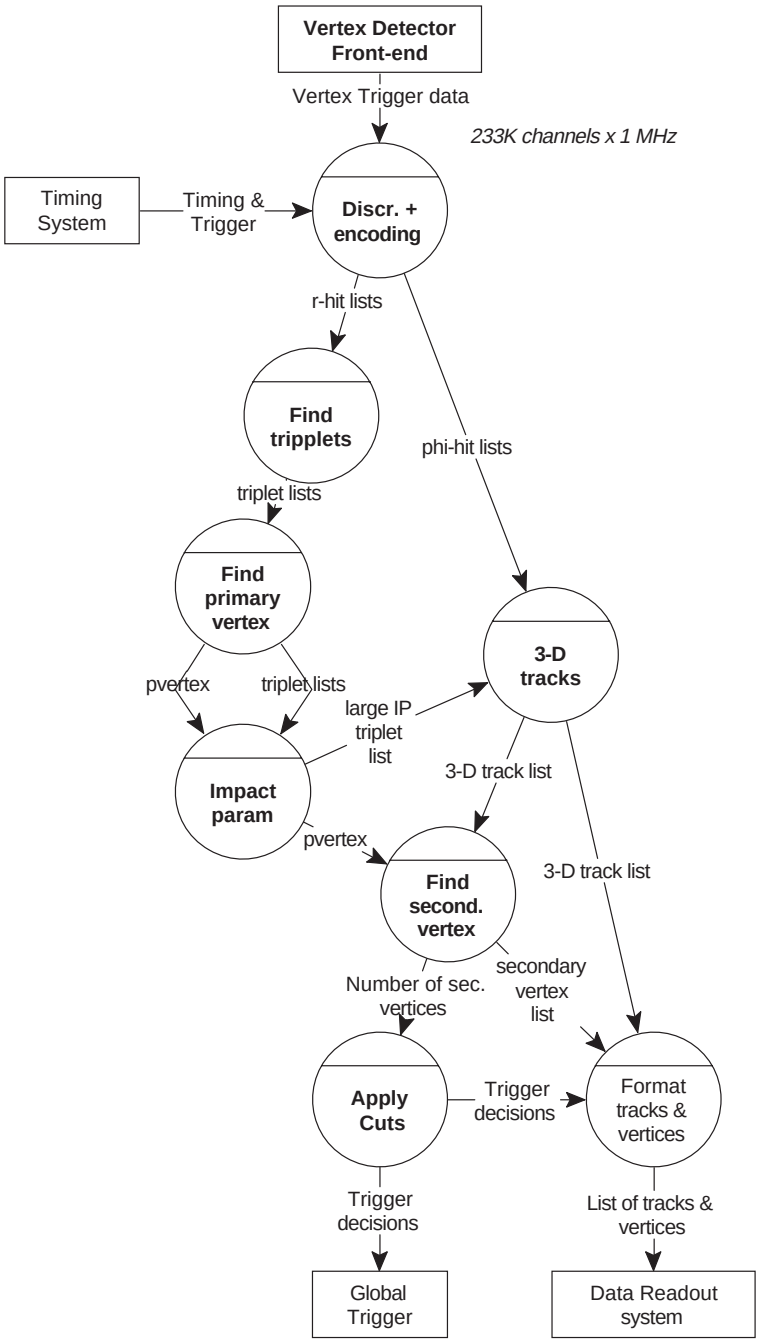

Figure 3: The vertex trigger algorithm.

- Calculation of the primary vertex position
- Impact parameter determination of all tracks
- 3D reconstruction of large impact parameter tracks
- Search for two track vertices separated from primary vertex

3.2 Track Finding Algorithm

The track search starts in the inner r-subsectors (12). Three colinear clusters in successive stations are used to define a track. The second r-cluster can either be in the inner or in the middle r-subsector. Only clusters with $r_1 < r_2 < r_3$ are accepted. In order to maintain a high track finding efficiency together with a low number of ghost tracks, the colinearity cut takes the measurement errors into account:

$$\begin{aligned} |r_3 - r_3^{\mathrm{extr}}| &< 3 \times \sigma \qquad (1)\\ \text{with} \quad r_3^{\mathrm{extr}} &= r_1 - z_1^r \times \frac{r_2 - r_1}{z_2^r - z_1^r} \\ \sigma^2 &= \left(\frac{z_3^r - z_2^r}{z_2^r - z_1^r}\sigma(r_1)\right)^2 + \left(\frac{z_3^r - z_1^r}{z_2^r - z_1^r}\sigma(r_2)\right)^2 + \sigma(r_3)^2 \end{aligned}$$

where z_i^r are the z-coordinates of the r-detectors and $\sigma(r_i)$ are the position resolutions.

The track parameters (slope m and crossing with r-axis b) are calculated using the first (z_1, r_1) and last cluster center (z_3, r_3):

$$m = \frac{r_3 - r_1}{z_3^r - z_1^r} \qquad (2)$$

$$b = r_1 - z_1^r \times m \qquad (3)$$

The silicon stations are scanned in positive z- and negative z-direction in order to reconstruct also tracks in backward direction for a better primary vertex determination.

Several segments of the same track can be found in different tripletts. A rejection process removes duplicate segments, leaving the one with a cluster closest to the beam.

Although on average only one hit per inner 30.5° sector is expected, the average number of clusters to be read out if there was at least one hit is 4.3. If there are clusters in station i and $i+1$, then in average 9.1 extrapolations to station $i+2$ have to be calculated. After removal of duplicate segments the mean number of forward tracks found is 36.

3.3 Primary Vertex finder

The estimate of the longitudinal coordinate of the primary vertex is made by histogramming the z-coordinates of two track vertices in $200\ \mu$m bins (Fig. 5):

$$z = -\frac{b_1 + b_2}{m_1 + m_2} \qquad (4)$$

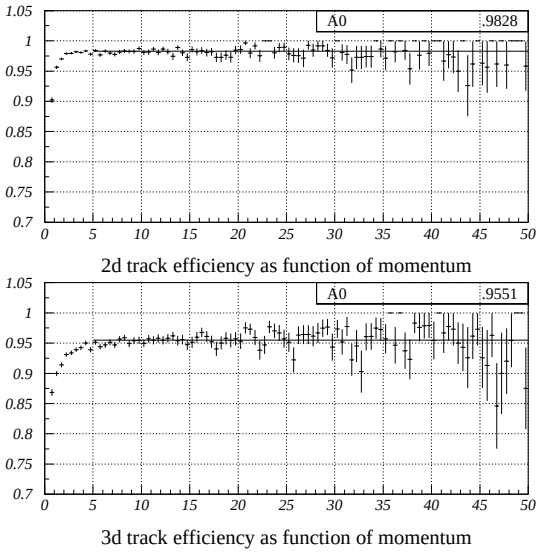

Figure 4: Efficiencies for the reconstruction of 2D and 3D tracks for particles which pass through the vertex detector as function of their momentum.

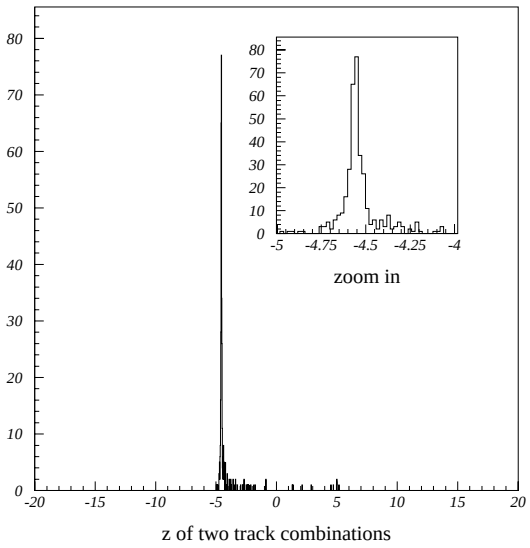

Figure 5: Histogram used to determine the z-position of the primary vertex. One event is shown.

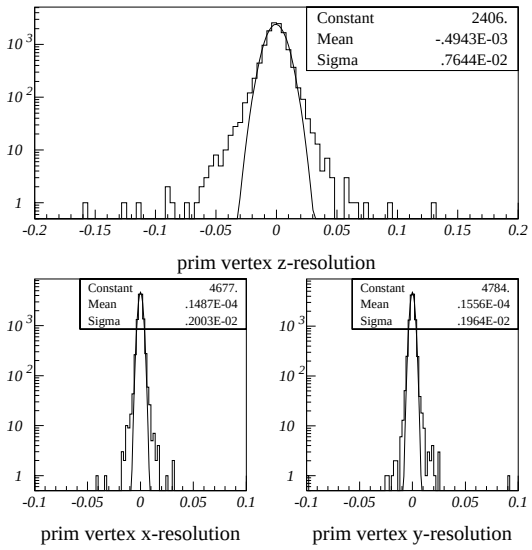

Figure 6: Resolution of the primary vertex vertex position obtained with the r-detectors only, in z (top), in x and y (bottom) for minimum bias events.

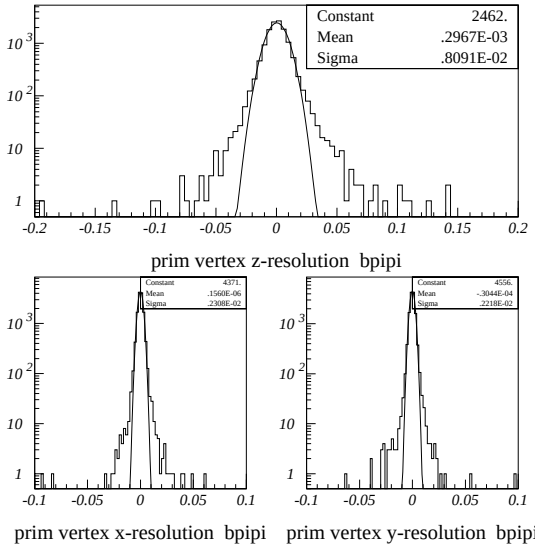

Figure 7: Resolution of the primary vertex vertex position obtained with the r-detectors only, in z (top), in x and y (bottom) for B-events.

Only tracks from opposite (± 2) ϕ-sectors are combined to select track pairs with large opening angles. On average, about 150 two track combinations exists in one event, but less than 100 combinations are enough for the desired precision. The weighted average of the bin with the maximal number of combinations and its two neighbours defines the z-position of the primary vertex with a resolution of 80 μm (Fig. 6). This procedure does not bias the z-position primary vertex of events with B-mesons (Fig 7). The tails in the distribution are very small considering the mean flight patch of a B-meson being 7 mm.

The transverse position of the vertex is obtained by histogramming for each ϕ-sector the distance d of the tracks to the z-axis at the position of the primary vertex. The x and y position of the primary vertex are determined with a precision of 20 μm (Fig. 6) from its ϕ-dependence:

$$d = x_p \times \sin(\phi) + y_p \times \cos(\phi) \tag{5}$$

3.4 Impact Parameter

For each 2D-track with a positive slope, the impact parameter with respect to the primary vertex is calculated:

$$\mathrm{IP} = -\frac{b - d + z_{\mathrm{pr.}} \times m}{\sqrt{m^2 + 1}} \tag{6}$$

where m,b and d are defined in equations 2, 3 and 5.

3.4.1 Pile-up

Pile-up events, which have two separated primary vertices are rejected by requiring an upper limit in the number of tracks with a large impact parameter to one of the primary vertices. Fig. 8 shows the number of tracks with an impact parameter larger than 500 μm. The difference is taken between the number of tracks with positive and negative impact parameters. The pile-up suppression is about 12.5 at an efficiency for single interactions of 99.9% when selecting events between -5 and 20 tracks.

3.4.2 Impact parameter probability

To select tracks with a significant impact parameter an estimate of the error on the impact parameter should be made. Since no momentum information is available the error is a function of the track length, the errors of the measured cluster positions and the extrapolation distance between the first measured point on the track and the primary vertex. Furthermore there is a weak correlation between the polar angle of the track and its momentum. Rather than parametrising the error, look-up tables are constructed for minimum bias events based on the parameters mentioned above. Given the lay-out of the vertex detector their can only be six different track length since all

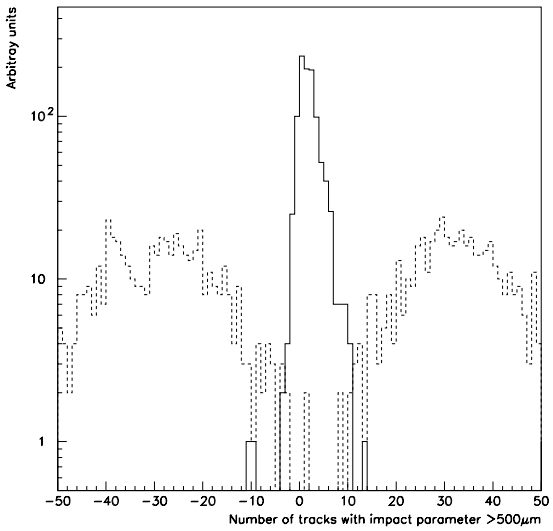

Figure 8: Pile-up rejection, plot shows number of tracks with $IP > 500\,\mu$m. The differnce is taken between the number of track with positve and negative impact parameters. Full line of for events with B-mesons, dashed line for pile-up events with two interactions.

tracks are defined as three hits in consecutive stations. The first hit on a track is always in the region with $40\,\mu$m strip pitch, hence only the strip pitch of the last hit is used to distinguish. For each of these 18 track classes the distance between primary vertex and first measured point is subdivided in ten bins. For each of these 180 track types the signed impact parameter distribution, where the B-meson is assumed to be produced with no transverse momentum, is transformed into a probability distribution. Only about half of the 180 track types actually exists. Fig. 9 shows 3 of these distributions. For each impact parameter the probability is defined as the fraction of tracks with an impact parameter larger than this value. Tracks with a probability smaller than 20% are selected for the 3D track reconstruction. For the examples in Fig. 9 this corresponds to effective impact parameter cuts of $125\,\mu$m, $225\,\mu$m and $2.5\,$mm.

3.5 3D Track Reconstruction

For the tracks with a large impact parameter (prob$< 20\%$), the ϕ cluster information of stations i and $i+1$ is now added. The extrapolated ϕ position of the track in station $i+2$ and the corresponding error is calculated:

$$\phi_3^{\mathrm{extr}} \approx \frac{z_3^\phi - z_1^\phi}{z_2^\phi - z_1^\phi} \times (\phi_2 - \phi_1) \times \frac{r_2}{r_3} + \phi_1 \qquad (7)$$

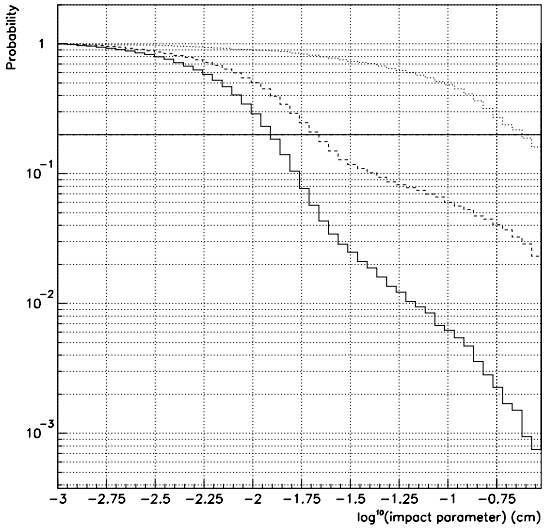

Figure 9: For each impact parameter the probability is defined as the fraction of track with an impact parameter larger than this value. The full-line shows the distributions for tracks which are 8 cm long, have a distance between the primary vertex and the first measured point of 7 cm, and have the last cluster on the track in the region with $40\ \mu$m strip pitch. Dashed (dotted) line for 20cm (8cm) long track, extrapolated over 70cm (20cm), and third hit in $40\ \mu$m ($60\ \mu$m) pitch region. The 20% probability cut has been indicated.

$$\sigma^2 = \left(\frac{z_3^\phi - z_1^\phi}{z_2^\phi - z_1^\phi}\right)^2 \left(\frac{r_2}{r_3}\left(\sigma(\phi_1)^2 + \sigma(\phi_2)^2\right) + \left(\frac{\phi_2}{r_3}\right)^2 + \left(\phi_2 \frac{r_2}{r_3^2}\sigma(r_3)\right)^2\right) + \sigma(\phi_1)^2 + \sigma(\phi_3)^2$$

and compared with the clusters found in station $i+2$:

$$|\phi_3^{\mathrm{extr}} - \phi_3| < 3 \times \sigma \tag{8}$$

The fact that the ϕ strips are rotated by a small angle, helps to resolve the hit ambiguities. Remaining ambiguities are solved by accepting only the combination with the smallest $x-y$ impact parameter. The reconstruction efficiencies obtained are about 98% for the 2D-tracks and 96% for the 3D tracks (Figure 4).

The 3D-track parameters are given by a direction vector $\vec{d}$ and a point X close to the first station hit by the track:

$$\vec{d} = \begin{pmatrix} \cos(\phi_1) & -\sin(\phi_1) & 0 \\ \sin(\phi_1) & \cos(\phi_1) & 0 \\ 0 & 0 & 1 \end{pmatrix} \times \begin{pmatrix} \frac{r_1 - r_3}{z_1^r - z_3^r} \\ \frac{\phi_3 - \phi_1}{z_3^\phi - z_1^\phi} \times \left(r_1 - [z_1^r - z_3^\phi] \times \frac{r_1 - r_3}{z_1^r - z_3^r}\right) \\ 1 \end{pmatrix}$$

$$X = \begin{pmatrix} \left(r_1 - [z_1^r - z_1^\phi]\right) \times \frac{r_1 - r_3}{z_1^r - z_3^r} \sin(\phi_1) \\ \left(r_1 - [z_1^r - z_1^\phi]\right) \times \frac{r_1 - r_3}{z_1^r - z_3^r} \cos(\phi_1) \\ z_1^\phi \end{pmatrix} \tag{9}$$

The direction vector is then normalized to 1.

3.6 Secondary vertex cuts

The algorithm aims to find secondary vertices which are separated significantly from the primary vertex. Since the momentum of the tracks is unknown, the error estimation of the impact parameters is derived from purely geometrical considerations, assuming straight tracks.

All 3D-tracks with an impact parameter (IP) in the rz plane less than 3 mm and a probability to originate from the primary vertex less than 20% (see above) are considered. This leads to about 13 combinations on average for minimum bias events. Fig. 10 shows the closest distance between a track and any other track in the event in space for tracks originating from a B (solid line) and for tracks in minimum bias events (dashed line). Only vertices with a distance between tracks smaller than $200\ \mu$m are accepted. Fig. 11 shows the number of secondary vertices with a distance to the primary vertex larger than 1.5 mm for $\mathrm{B} \to \pi\pi$ events (solid line) and for minimum bias events (dashed line). Each secondary vertex is assigned the smallest impact probability of its track pair. These probabilities are multiplied to form a total event probability.

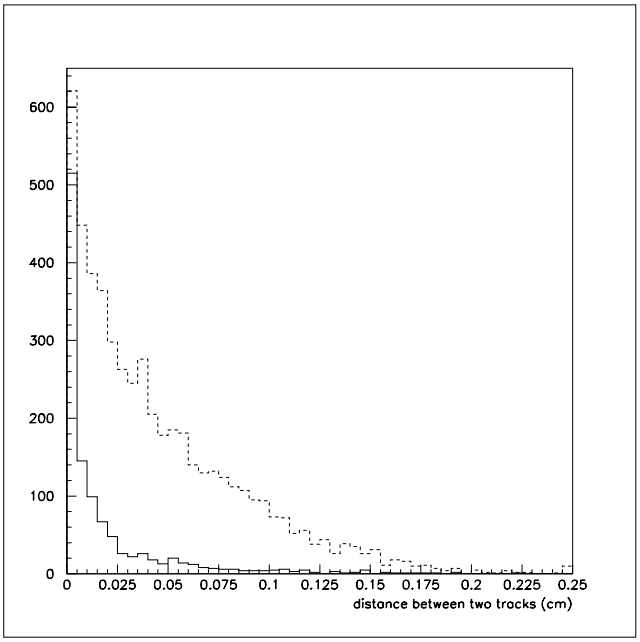

Figure 10: The closest distance between a track and any other track in the event in space for tracks originating from a B (solid line) and for tracks in minimum bias events (dashed line) is shown.

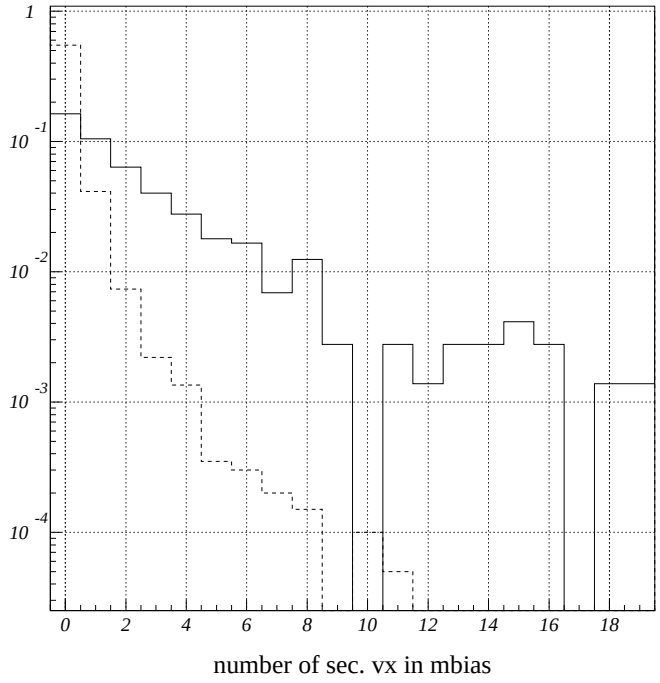

Figure 11: The number of secondary vertices with a significant distance to the primary vertex for $\mathrm{B} \rightarrow \pi\pi$ events (solid line) and for minimum bias events (dashed line) is shown.

Table 2: Statistic of the different sources of tracks with large impact parameters in minimum bias events.

origin	contribution
measurement errors†	48.1%
ghost tracks	14.1%
photon conversion	1.6%
nuclear interaction	0.4%
$\mathrm{K_s}$ decays	27.1%
other strange particles	5.4%
charm and tau decays	2.5%
beauty particles	0.7%

† includes multiple scattering

3.6.1 Source of large impact parameter tracks

The sources of tracks with a large impact parameter are summarized in Table 2. The dominant contribution are low momentum tracks (Figure 12,13) which can be removed in a later stage of the trigger (L2), when momentum information of the tracking stations becomes available.

3.7 Performance

The Level-1 trigger algorithm is being tailored to meet the selection criteria proposed for use off-line in the reconstruction of B-mesons. The decay mode $\mathrm{B} \to \pi\pi$ is being used to demonstrate its performance, since this is one of the most demanding modes due to its low final state multiplicity and the absence of sub-mass constraints. The $\mathrm{B} \to \pi\pi$ decay mode has a vertex with only two charged particles, and hence only two tracks will be required per vertex. However using the associated B-meson decay more than one vertex can be demanded per event in order to improve the suppression of minimum bias events.

In order to evaluate how well the vertex trigger performs for B events which can be reconstructed off-line, the B-events have been subjected to the following off-line cuts:

- The $\mathrm{B} \to \pi\pi$ has a decay length larger than 1.5 mm.
- Both the pions from $\mathrm{B} \to \pi\pi$ measured in at least two silicon stations, and have a momentum measurement from the spectrometer.
- $\mathrm{IP}/\sigma(\mathrm{IP}) > 3$ for both pions in the $\mathrm{B} \to \pi\pi$ decay.
- at least one charged track of the other B is seen in the spectrometer.

Since the final Level-0 trigger cuts were not defined at the time of this note, no requirements on Level-0 are applied.

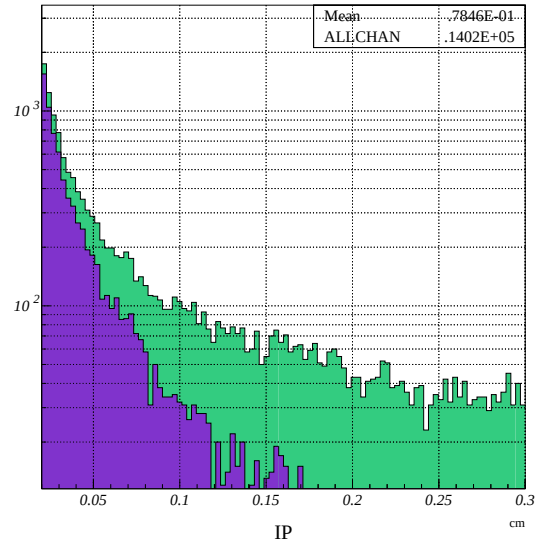

Figure 12: Impact parameter distribution of 2D-tracks in minimum bias events. The dark area represents the contribution of tracks which originate from the primary vertex.

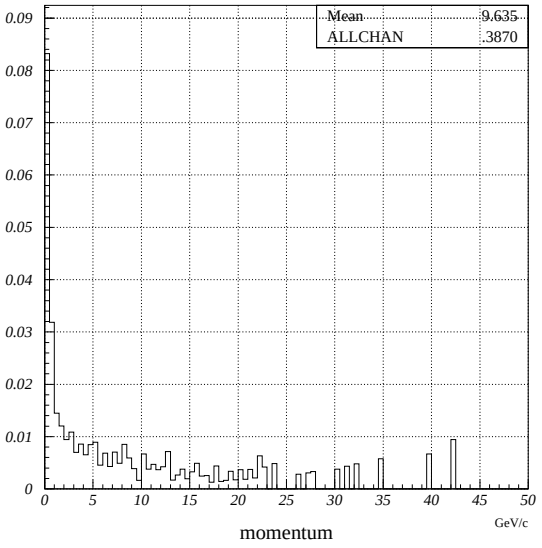

Figure 13: Percentage of tracks with large impact parameter as function of the momentum. Main contribution comes from low momentum tracks which have large multiple scattering.

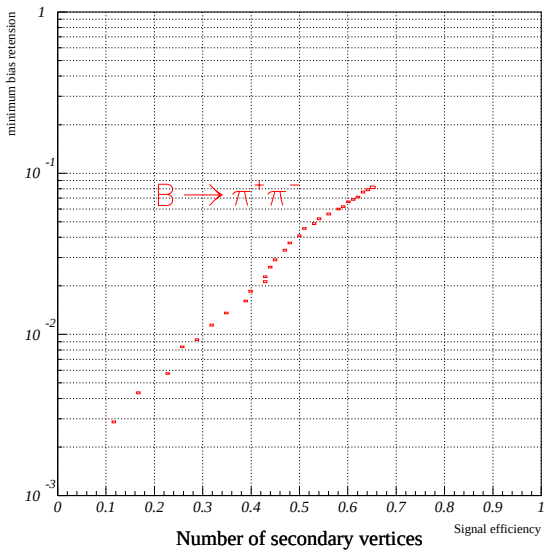

Figure 14: The retention of minimum bias events against the trigger efficiency of $\mathrm{B} \rightarrow \pi\pi$ events .

By varying the cut on the distance between primary and secondary vertices, and on the number of secondary vertices and the total event probability as defined above the trigger efficiency can be determined as a function of the retention of minimum bias events (Fig. 14). A 4% minimum bias retention is achieved together with an 50% efficiency for $\mathrm{B} \rightarrow \pi\pi$.

3.8 Noise Study

Because of the high radiation level, we expect a decrease in the signal over noise ratio in the silicon detector [2]. The online cluster finding algorithm can either be adapted to keep a constant fraction of ghost clusters at the expense of a loss in efficiency (see [3]), or a balance can be found increasing the number of ghost clusters, but minimizing the loss in efficiency. The consequence of this increase in noise is discussed here.

The performance of the L1 trigger was studied under different noise situations, from no noise up to noise levels after several times the expected fluence for one year of operation. The relationship of S/N and the number of noise clusters and efficiency have been taken from [4]. A constant single hit efficiency of 99.7% has been assumed.

The expected noise has been calculated while keeping the single hit efficiency constant. The results are summarized in table 3. One year of running would correspond to about 1×10^{14} particles/cm^{-2}. A 10% loss in signal efficiency and a 10% increase in the minimum bias retension is observed after a dose which corresponds to five year running.

Table 3: Summary of the effect of noise on the L1 performance. Results are based on 1000 events minimum bias and 1000 events $\mathrm{B} \to \pi^+\pi^-$ with different levels of noise overlayed.

integrated fluence [10^{14} particles/cm^{-2}]	0	3	4	4.2	4.6	5.3
$\langle r \rangle$ clusters	307.4	338.5	385.3	415.5	462.3	632.6
$\langle \phi \rangle$ clusters	296.4	325.8	368.9	397.7	441.4	605.9
2D track efficiency	98.1%	98.0%	98.0%	97.5%	97.8%	96.6%
3D track efficiency	95.7%	95.7%	95.7%	95.2%	95.3%	93.9%
2D ghosts	3.4%	5.4%	7.8%	11.6%	15.3%	25.6%
3D ghosts	17.5%	17.7%	17.3%	20.3%	21.1%	28.0%
passing L1	4.1%	4.4%	4.1%	4.3%	4.5%	4.5%
$\mathrm{B} \to \pi^+\pi^-$ efficiency	51.7%	49.2%	50.8%	52.5%	49.2%	46.7%

3.9 Effect of detector mis-alignments

Possible mis-alignments of the vertex detector had been studied in a separate note [5].

References

[1] D. Steele, LHCb/98-004, TRAC.

[2] H. Dijkstra, LHCb/98-009, DAQ.

[3] O. Cooke, LHCb/97-023, TRAC.

[4] P. Koppenburg, LHCb/97-020, TRAC.

[5] M. Koratzinos and T. Ruf, LHCb/98-012, TRIG.